Large Curvature Tunneling Effects Reveal Concerted Hydrogen Exchange Rates in Cyclic Hydrogen Fluoride Clusters Comparable to Carboxylic Acid Dimers

Thomas Loerting, Klaus R. Liedl,* and Bernd M. Rode

Contribution from the Department of Theoretical Chemistry, Institute of General, Inorganic and Theoretical Chemistry, University of Innsbruck, Innrain 52a, A-6020 Innsbruck, Austria

Received August 11, 1997. Revised Manuscript Received November 12, 1997

Abstract: Reaction rate constants for the concerted proton transfer in cyclic hydrogen fluoride clusters obtained by using a variational transition state theory approach with high-level data at three stationary points and with interpolated corrections based on semiempirical Hamiltonians specially parametrized for these systems—MP2/6-311++G(3df,3pd)///PM3-SRP—are reported. For the first time multidimensional tunneling is included in the large curvature limit. The corresponding small curvature limit is benchmarked against higher level calculations. The ridge of the reaction swath is defined in a general way and serves together with an estimate of the barrier width as a validation of the potential energy hypersurfaces. Recent experimental and theoretical results concerning carboxylic acids, whose hypersurfaces are found to be very similar to those of the HF clusters, underline the relevancy of the investigated concerted proton exchange motion. A reaction rate constant $k(300\ \mathrm{K}) = 2.86 \times 10^9\ \mathrm{s}^{-1}$ is found for $(HF)_5$, which is similar to carboxylic acid dimers, whose experimental $k(300\ \mathrm{K})$ lie near $10^{10}\ \mathrm{s}^{-1}$.

1. Introduction

Gaseous hydrogen fluoride clusters are well-known components of hydrofluoric acid vapor[1,2] and serve, not only due to their planarity, as highly symmetric (i.e., C_{nh} for minimum structures and D_{nh} for transition states) models to establish hydrogen-bonding concepts that should be extensible to more complex systems such as water clusters or even condensed biomolecules containing no symmetry elements, as base pairs in DNA or RNA. This study focuses on the clockwise−counterclockwise (cw-ccw) isomerization of cyclic $(HF)_n$ ($n = 3-5$) clusters,[1,3−7] where n hydrogen atoms simultaneously move from their covalent fluorine partners (hydrogen bond donor) to the neighboring fluorine atoms (hydrogen bond acceptor) in a way that the orientation of the hydrogen fluoride monomers is reversed frequently between cw and ccw. Extensive theoretical and experimental studies are available for gaseous, solid, and solvated species showing such a multiple proton and deuteron transfer, e.g. in carboxylic acid dimers,[8−14] pure methanol,[15] acetic acid/methanol,[16,17] solid pyrazoles,[18,19] amidine dimers,[13,20,21] oxalamidines,[22] water clusters,[23,24] and porphyrines.[25] Since the abundance of $(HF)_n$ ($n = 2-8$) complexes in the gas phase has been a familiar fact for a long time,[26,27] experimental investigations have been performed exhaustively,[1,2,28−32] which

* Address correspondence to this author.

(1) Quack, M.; Schmitt, U.; Suhm, M. A. *Chem. Phys. Lett.* **1993**, *208*, 446−452.
(2) Suhm, M. A. *Ber. Bunsen.-Ges. Phys. Chem.* **1995**, *99*, 1159−1167.
(3) Gaw, J. F.; Yamaguchi, Y.; Vincent, M. A.; Schaeffer, H. F., III *J. Am. Chem. Soc.* **1984**, *106*, 3133−3138.
(4) Heidrich, D.; Köhler, H.-J.; Volkmann, D. *Int. J. Quantum Chem.* **1985**, *27*, 781−786.
(5) Karpfen, A. *Int. J. Quantum Chem., Quantum Chem. Symp.* **1990**, *24*, 129−140.
(6) Komornicki, A.; Dixon, D. A.; Taylor, P. R. *J. Chem. Phys.* **1992**, *96*, 2920−2925.
(7) Quack, M.; Suhm, M. A. Potential Energy Hypersurfaces For Hydrogen Bonded Clusters $(HF)_N$. In *Conceptual Trends in Quantum Chemistry*; Vol. III, *Conceptual Perspectives in Quantum Chemistry*; Kluwer Publishing Co.: Dordrecht, 1997; pp 417−467.
(8) Meier, B. H.; Graf, F.; Ernst, R. R. *J. Chem. Phys.* **1982**, *76*, 767−774.
(9) Stöckli, A.; Meier, B. H.; Kreis, R.; Meyer, R.; Ernst, R. R. *J. Chem. Phys.* **1990**, *93*, 1502−1520.
(10) Meyer, R.; Ernst, R. R. *J. Chem. Phys.* **1990**, *93*, 5518−5532.
(11) Heuer, A.; Haeberlen, U. *J. Chem. Phys.* **1991**, *95*, 4201−4214.
(12) Kim, Y. *J. Am. Chem. Soc.* **1996**, *118*, 1522−1528.
(13) Lim, J.-H.; Lee, E. K.; Kim, Y. *J. Phys. Chem.* **1997**, *101*, 2233−2239.
(14) Brougham, D. F.; Horsewill, A. J.; Jenkinson, R. I. *Chem. Phys. Lett.* **1997**, *272*, 69−74.
(15) Gerritzen, D.; Limbach, H. H. *Ber. Bunsen-Ges. Phys. Chem.* **1981**, *85*, 527−535.
(16) Limbach, H. H.; Seiffert, W. *J. Am. Chem. Soc.* **1980**, *102*, 538−542.
(17) Gerritzen, D.; Limbach, H. H. *J. Am. Chem. Soc.* **1984**, *106*, 869−879.
(18) Smith, J. A. S.; Wehrle, B.; Aguilar-Parrilla, F.; Limbach, H. H.; Foces-Foces, M. C.; Hernandez Cano, F.; Elguero, J.; Baldy, A.; Pierrot, M.; Khurshid, M. M. T.; Larcombe-McDouall, J. B. *J. Am. Chem. Soc.* **1989**, *111*, 7304−7312.
(19) Aguilar-Parrilla, F.; Scherer, G.; Limbach, H. H.; Foces-Foces, M. C.; Hernandez Cano, F.; Smith, J. A. S.; Toiron, C.; Elguero, J. *J. Am. Chem. Soc.* **1992**, *114*, 9657−9659.
(20) Meschede, L.; Limbach, H. H. *J. Phys. Chem.* **1991**, *95*, 10267−10280.
(21) Männle, F.; Wawer, I.; Limbach, H. H. *Chem. Phys. Lett.* **1996**, *256*, 657−662.
(22) Scherer, G.; Limbach, H. H. *J. Am. Chem. Soc.* **1994**, *116*, 1230−1239.
(23) Garrett, B. C.; Melius, C. F. In *Theoretical and Computational Models for Organic Chemistry*; NATO ASI Series C 339; Formosinho, S. J.; et al., Eds.; Kluver Academic: The Netherlands, 1991; pp 35−54.
(24) Liedl, K. R.; Sekusak, S.; Kroemer, R. T.; Rode, B. M. *J. Phys. Chem.* **1997**, *101*, 4707−4716.
(25) Braun, J.; Limbach, H. H.; Williams, P. G.; Morimoto, H.; Wemmer, D. E. *J. Am. Chem. Soc.* **1996**, *118*, 7231−7232.
(26) Hindermann, D. K.; Cornwell, C. D. *J. Chem. Phys.* **1968**, *48*, 2017−2025.
(27) Mackor, E. L.; MacLean, C.; Hilbers, C. W. *Rec. Trav. Chim. Pays-Bas* **1968**, *87*, 655−672.

S0002-7863(97)02799-6 CCC: $15.00 © 1998 American Chemical Society
Published on Web 01/03/1998

is reflected in the number of theoretical publications.[5−7,33−37] Particularly, structure, thermodynamics, kinetics, rovibrational spectra, and magnetic properties are interesting and extensively treated questions in terms of spectroscopy as well as in terms of computational methods.

This study concentrates on the dynamical behavior of $(HF)_3$−$(HF)_5$ aggregates. $(HF)_2$ is not considered, as its mechanism of hydrogen exchange is different from the higher oligomers.[38,39] A determination of reliable proton exchange rates is performed by examining several different aspects: First, a basis transformation of the reactant's geometry to the normal mode basis of the transition state is performed. The reactant's coefficient of the reaction coordinate direction at the saddle point is related to the barrier width. Second, the ridge of the reaction swath[24] is defined in a systematic and generally applicable way. It serves as a confirmation of the shape of the potential energy surface (PES) and shows the indisputable need for the consideration of direct corner cutting effects. Third, variational transition state theory with interpolated corrections (VTST-IC)[40−42] including quantum-mechanical multidimensional tunneling calculations in the small and large curvature case[43−45] is applied as a function of temperature. This approach is used to obtain the rate constants based on the MP2/6-311++G(3df,3pd) description of minima and the saddle point with interpolated corrections by semiempirical Hamiltonians specially parametrized for each individual system (PM3-SRP).[46,47] The concept of SRP, which is an abbreviation for specific reaction parameters, already has been successfully applied by other groups in the past[12,41,42,48,49] to achieve useful semiempirical hypersurfaces.

Finally, a comparison to calculations of carboxylic acid dimers is performed, where experimental investigations of rate constants are available.[8,9,11,14] The experimental rate constants of carboxylic acid dimers were all found to be between 2.0×10^{10} s^{-1} and 1.8×10^{11} s^{-1} with natural isotopic substitution and between 2.5×10^{9} s^{-1} and 1.5×10^{10} s^{-1} for fully deuterated complexes, and therefore allow a validation of our predictions.

2. Methods and Calculations

2.1. Theory. Widely used approaches to calculate reaction rate constants are collision theory[50] and transition state theory (TST).[43,51−53] We have chosen an advanced variant of the latter approach: In TST the reaction rate is obtained a priori only from information about the reactants and the transition state or, more generally spoken, the bottleneck of the reaction. The products themselves do not contribute to the evaluation of the rate constant k, as a major part of theory is the "no recrossing assumption", i.e., each trajectory that reaches the transition state (TS) on the reaction path is assumed to be converted to products and trapped there on the PES. This assumption is not fulfilled in reality, and trajectories in fact can recross the highest point several times. Therefore the TST rate constant provides only an upper limit for the experimental rate constant. By varying the location of the hypersurface, dividing reactants from products, and minimizing the computed k and thus minimizing recrossing, this error can be reduced drastically. This approach is called variational transition state theory (VTST) and can provide considerably better agreement with experiment than pure TST.[43,52]

Nevertheless, this strategy still fails to describe nonclassical trajectories tunneling through a barrier. Especially when the curvature of the PES near the transition state is large, the rate constants without inclusion of quantum-mechanical tunneling methods can be considerably wrong.[43,52] The amount of tunneling is taken into account by multiplying the pure variational rate constant $k^{CVT}(T)$ with a transmission coefficient κ, where the superscript CVT indicates that a canonical ensemble was assumed for the calculation. Depending on the curvature of the minimum energy path (MEP), which is defined as the steepest descent path in mass-weighted Cartesian coordinates connecting saddle points and minima,[54] different quantum-mechanical methods can be used to take into account the nuclei's quantum properties. The minimum energy path semiclassical adiabatic ground state (MEPSAG) method is appropriate, if the tunneling path coincides with the MEP.[55] It is also called the zero curvature method (ZCT), because a one-dimensional, straight reaction path is assumed. As the reaction path is in fact curved, tunneling is assumed to occur on the path defined by the classical turning points on the concave side of the MEP ("anti-bobsleigh effect"). This type of calculation is called the centrifugal-dominant small curvature semiclassical adiabatic ground state (CD-SCSAG) method, a small curvature tunneling (SCT) approach.[45] For light atom transfer reactions the reaction path curvature is very large and the centrifugal dominant approximation breaks down. In the large curvature ground-state approximation, version 3 (LCG3),[43,44] a large curvature tunneling (LCT) method, it is assumed that the short distance between tunneling start and end point forces the system to take straight paths between these two points. This approximation includes contributions from all straight-line tunneling paths with equal kinetic energy in reaction coordinate motion at the pre- and post-tunneling configuration coordinate by using a quasiclassical distribution function to average over paths with different end points. Especially at low temperatures, κ can deviate from one (i.e., no tunneling) considerably and change calculated rate constants by several orders of magnitude.

(28) Janzen, J.; Bartell, L. S. *J. Chem. Phys.* **1969**, *50*, 3611−3618.
(29) Suhm, M. A.; Farrell, J. T., Jr.; Ashworth, S. H.; Nesbitt, D. J. *J. Chem. Phys.* **1993**, *98*, 5985−5989.
(30) Huisken, F.; Kaloudis, M.; Kulcke, A.; Laush, C.; Lisy, J. M. *J. Chem. Phys.* **1995**, *103*, 5366−5377.
(31) Luckhaus, D.; Quack, M.; Schmitt, U.; Suhm, M. A. *Ber. Bunsen-Ges. Phys. Chem.* **1995**, *99*, 457−468.
(32) Quack, M.; Schmitt, U.; Suhm, M. A. *Chem. Phys. Lett.* **1997**, *269*, 29−38.
(33) Hancock, G. C.; Truhlar, D. G. *J. Chem. Phys.* **1989**, *90*, 3498−3505.
(34) Wales, D. J. *J. Am. Chem. Soc.* **1993**, *115*, 11191−11201.
(35) Karpfen, A.; Yanovitskii, O. *J. Mol. Struct. (THEOCHEM)* **1994**, *314*, 211−227.
(36) Liedl, K. R.; Kroemer, R. T.; Rode, B. M. *Chem. Phys. Lett.* **1995**, *246*, 455−462.
(37) Märker, C.; Schleyer, P. v. R.; Liedl, K. R.; Ha, T.-K.; Quack M.; Suhm, M. A. *J. Comput. Chem.* **1997**, *18*, 1695−1719.
(38) Kofranek, M.; Lischka, H.; Karpfen, A. *Chem. Phys.* **1988**, *99*, 137−153.
(39) Quack, M.; Suhm, M. A. *J. Chem. Phys.* **1991**, *95*, 28−59.
(40) Gonzalez-Lafont, A.; Truong, T. N.; Truhlar, D. G. *J. Chem. Phys.* **1991**, *95*, 8875−8894.
(41) Hu, W.-P.; Liu, Y. P.; Truhlar, D. G. *J. Chem. Soc., Faraday Trans.* **1994**, *90*, 1715−1725.
(42) Corchado, J. C.; Espinosa-Garcia, J.; Hu, W.-P.; Rossi, I.; Truhlar, D. G. *J. Phys. Chem.* **1995**, *99*, 687−694.
(43) Truhlar, D. G.; Isaacson, A. D.; Garrett, B. C. Generalized Transition State Theory. In *Theory of Chemical Reaction Dynamics*; Baer, M., Ed.; CRC Press: Boca Raton, FL, 1985; pp 65−137.
(44) Garrett, B. C.; Joseph, T.; Truong, T. N.; Truhlar, D. G. *Chem. Phys.* **1989**, *136*, 271−283.
(45) Liu, Y.-P.; Lynch, G. C.; Truong, T. N.; Lu, D.-h.; Truhlar, D. G.; Garrett, B. C. *J. Am. Chem. Soc.* **1993**, *115*, 2408−2415.
(46) Stewart, J. J. P. *J. Comput. Chem.* **1989**, *10*, 209−220.
(47) Stewart, J. J. P. *J. Comput. Chem.* **1989**, *10*, 221−264.
(48) Nguyen, K. A.; Rossi, I.; Truhlar, D. G. *J. Chem. Phys.* **1995**, *103*, 5522−5530.
(49) Rossi, I.; Truhlar, D. G. *Chem. Phys. Lett.* **1995**, *233*, 231−236.
(50) Billing, G. D.; Mikkelsen, K. V. Collisional Approach. In *Introduction to Molecular Dynamics and Chemical Kinetics*; John Wiley & Sons, Inc.: Copenhagen and Arhus, 1996; pp 18−24.
(51) Kreevoy, M. M.; Truhlar, D. G. Transition State Theory. In *Investigation of Rates and Mechanisms of Reactions*; Bernasconi, C. F., Ed.; John Wiley & Sons, Inc.: New York, 1986; pp 13−95.
(52) Tucker, S. C.; Truhlar, D. G. Dynamical Formulation of Transition State Theory: Variational Transition States and Semiclassical Tunneling. In *New Theoretical Concepts for Understanding Organic Reactions*; NATO ASI Series C 267; Bertrán, J., Csizmadia, I. G., Eds.; Kluwer: Dordrecht, The Netherlands, 1989; pp 291−346.
(53) Truhlar, D. G.; Garrett, B. C.; Klippenstein, S. J. *J. Phys. Chem.* **1996**, *100*, 12771−12800.
(54) Miller, W. H.; Handy, N. C.; Adams, J. E. *J. Chem. Phys.* **1980**, *72*, 99−112.
(55) Garrett, B. C.; Truhlar, D. G.; Grev, R. S.; Magnuson, A. W. *J. Phys. Chem.* **1980**, *84*, 1730−1748.

Depending on the nature of the PES, κ can also vary strongly with the level of sophistication of tunneling inclusion. For a strongly bent PES the differences between κ^{ZCT}, κ^{SCT}, and κ^{LCT} can rise to several orders of magnitude at room temperature.[40,42] One should be aware that calculations can only lead to results comparable to experiment for a wide range of temperatures, when the provided PES is accurate enough. Due to limitations in resources, it is hardly possible to calculate the whole PES in terms of ab initio calculations and it is, therefore, necessary to find a cheaper method for a good description of the hypersurface as described in the following sections. The detailed mathematical procedures and computational formulas are discussed elsewhere.[43,52]

2.2. Potential Energy Hypersurface. To have a computationally low demanding method available, which reproduces high-quality (MP2/6-311++G(3df,3dp)) ab initio structural and electronic data at three stationary points on the potential energy hypersurface as well as possible, the common PM3 Hamilton operator[46,47] was reparametrized. This parameter optimization was carried out with use of GAucsd1.4,[56] a global optimization strategy,[49] on the basis of a genetic algorithm.[57] The fine-tuning was performed with an adapted implementation of a Levenberg−Marquardt[58] local minimization method. The necessary structural, vibrational, and thermodynamical data were obtained from an interface to MOPAC5.05mn[59] by applying the PM3 Hamiltonian with user defined specific reaction parameters (PM3-SRP).

For the determination of points on the ridge of the reaction swath,[24] a basis set transformation of the reactant's and product's coordinates to the normal mode basis of the transition state[36] was performed with the aid of the matrix manipulation tool MATLAB.[60] For this purpose rotational and translational contributions had to be removed beforehand. For a validation of the PM3-SRP description between stationary point single point energies for structures on the ridge of the reaction swath, geometries of first-order transition states (TS) and minima on the potential energy hypersurface were calculated with use of the GAUSSIAN 94[61] series of programs applying the hybrid density functional theory Becke3LYP[62] and 6-31+G(d) as the basis set.[63−65] Compared to MP2/6-311++G(3df,3dp), this method consumes only a small fraction of computation time and reproduces the MP2 results quite well. The barrier was found to be consistently 2.5−3.5 kcal/mol too low, while the zero-point corrections agree within 0.5 kcal/mol. Geometric predictions are reproduced within 0.04 Å and less than 2.0° for minima as well as for transition states. All hybrid density functional theory normal modes deviate less than 10% or 50 cm^{-1} from the MP2 theory result. For the validation of the PES it therefore seems to be legitimate to calculate points on the ridge of the reaction swath with this cheaper approach. Finally, evidence that the chosen basis set is sufficient can be found in the fact that the ridge of the reaction swath curves calculated at the B3LYP/6-311++G(3df,3dp)[24] level of theory coincide with those of the B3LYP/6-31+G(d) level quite well.

2.3. Dynamics. Rate constants k and transmission coefficients κ were obtained by using the program package MORATE7.2,[66] applying a dual-level dynamics method called MP2/6-311++G (3df,3dp)///PM3-SRP, where "///" means "with interpolated corrections at" and is equivalent to VTST-IC.[51,52,67] Reaction paths were calculated starting from the TS (by definition at $s = 0$ Bohr) up to a distance of $s = 3.5$ Bohr for $(HF)_3$, $s = 3.0$ Bohr for $(HF)_4$, and $s = 3.5$ Bohr for $(HF)_5$ away from the corresponding saddle point geometry in both directions. The reaction coordinate s is given in isoinertial coordinates with a scaling factor of 1 amu. The variational approach showed that the bottleneck (generalized TS) of all systems at the computed temperatures stays at the transition state structure at $s = 0$ Bohr. The dynamical procedure uses accurate MP2/6-311++G(3df,3dp) ab initio data at three extrema, namely at the D_{nh} transition state structure and the two C_{nh} minima. The interpolation between these extrema is based on the logarithm of ratios (ICL)[68] between the high-level ab initio and the low-level PM3-SRP data. Hence, the Born−Oppenheimer potential along the minimum energy path V_{MEP} (s), the vibrational frequencies ω(s), and the moment-of-inertia determinants $|\mathbf{I}(s)|$ were corrected by applying an Eckart functional form, using the low-level (PM3-SRP) electronic structure data and providing an explicit match at the three stationary points. This procedure ensures that the high-level data are used, especially the energy difference between C_{nh} and D_{nh} structures, where they are available and that the low-level information along the whole range of the reaction path is smoothly fitted to the direct interpolation as a function of s. The range parameter L for the Eckart fit was gained from a four-point fit, yielding 0.362297, 0.345629, and 0.359504 Bohr for tri-, tetra-, and pentamer, respectively.[41]

The transmission coefficients κ for the description of the effect of semiclassical multidimensional tunneling and nonclassical reflection were obtained by using variational transition state theory with interpolated corrections (VTST-IC),[51,52,69,67] using the CD-SCSAG and LCG3 methods.[52] On the minimum energy path some frequencies−1 degenerate pair, 2 single ones, and 2 pairs for tri-, tetra-, and pentamer, respectively−had small "imaginary" values (i.e., negative force constants) and therefore required special treatment. These small "imaginary" frequencies were handled in terms of interpolated VTST of zeroth-order (IVTST-0),[40] which renders them positive along the whole range of reaction coordinate motion, giving the possibility of including their zero-point energy in the adiabatic ground-state potential V_a^G (s). The normal modes were connected, as suggested previously,[24,70] by providing maximal overlap between two successive grid points on the reaction path, a method now also implemented in POLYRATE7.2 (REORDER keyword). The step size on the reaction path was 5.0×10^{-4} Bohr in an isoinertial coordinate system, where a scaling factor of 1.0 amu was used for convenience.

3. Parametrization

3.1. Strategy. The PM3 parametrization strategy was worked out with the smallest oligomer, namely $(HF)_3$. A crucial step for the theoretical prediction of the experimental rate of hydrogen exchange is to provide a reasonable barrier (i.e., width and height) and frequencies at computationally low demands. MP2/6-311++G(3df,3dp) data were taken as reference.[24,37] (The combination of all properties will be referred to as "configurations" for future use.)

These reference results, most important the barrier height, are in excellent agreement with the highest quality estimates available. For example, the 18.73 kcal/mol (MP2/6-311++G(3df,3dp)) value for the trimer's barrier height agrees quite well with 18.61 kcal/mol (MP2/

(56) Schraudolph, N.; Grefenstette, J. *GAucsd 1.4*. University of California, San Diego, 1992.

(57) Goldberg, D. E. Genetic algorithms in search, optimization and machine learning. In *Physical Chemistry*; Addison-Wesley: Reading, 1989.

(58) Press, W. H.; Vetterling, W. T.; Teukolsky, S. A.; Flannery, B. P. Modeling of Data. In *Numerical Recipes in C, 2nd ed.*; University Press: Cambridge, 1995; pp 656−699.

(59) Stewart, J. J. P.; Rossi, I.; Hu, W.-P.; Lynch, G. C.; Liu, Y.-P.; Truhlar, D. G. *MOPAC-version 5.05mn*; University of Minnesota, Minneapolis, 1995.

(60) *MATLAB 4.1*; Math Works Inc., Natick, 1993.

(61) Frisch, M. J.; Trucks, G. W.; Schlegel, H. B.; Gill, P. M. W.; Johnson, B. G.; Robb, M. A.; Cheeseman, J. R.; Keith, T. A.; Petersson, G. A.; Montgomery, J. A.; Raghavachari, K.; Al-Laham, M. A.; Zakrzewski, V. G.; Ortiz, J. V.; Foresman, J. B.; Cioslowski, J.; Stefanov, B. B.; Nanayakkara, A.; Challacombe, M.; Peng, C. Y.; Ayala, P. Y.; Chen, W.; Wong, M. W.; Andres, J. L.; Replogle, E. S.; Gomperts, R.; Martin, R. L.; Fox, D. J.; Binkley, J. S.; Defrees, D. J.; Baker, J.; Stewart, J. P.; Head-Gordon, M.; Gonzalez, C.; Pople, J. A. *Gaussian 94, Revision D.1*; Gaussian, Inc.: Pittsburgh, PA, 1995.

(62) Becke, A. D. *J. Chem. Phys.* **1993**, *98*, 5648−5652.

(63) Krishnan, R.; Binkley, J. S.; Seeger, R.; Pople, J. A. *J. Chem. Phys.* **1980**, *72*, 650−654.

(64) Frisch, M. J.; Pople, J. A.; Binkley, J. S. *J. Chem. Phys.* **1984**, *80*, 3265−3269.

(65) Gill, P. M. W.; Johnson, B. G.; Pople, J. A.; Frisch, M. J. *Chem. Phys. Lett.* **1992**, *197*, 499−505.

(66) Chuang, Y.-Y.; Hu, W.-P.; Lynch, G. C.; Liu, Y.-P.; Truhlar, D. G. *MORATE-version 7.2*; University of Minnesota, Minneapolis, 1997.

(67) Truhlar, D. G. Direct Dynamics Method for the Calculation of Reaction Rates, In *The Reaction Path in Chemistry: Current Approaches and Perspectives*; Heidrich, D., Ed.; Kluwer: Dordrecht, 1995; pp 229−255.

(68) Chuang, Y.-Y.; Truhlar, D. G. *J. Phys. Chem. A* **1997**, *101*, 3808−3814.

(69) Benderskii, V. A.; Makarov, D. E.; Wight, C. A. *Advances in Chemical Physics*; Vol. LXXXVIII, Chemical Dynamics at Low Temperatures, John Wiley & Sons, Inc.: New York, 1994.

(70) Sekusak, S.; Liedl, K. R.; Rode, B. M.; Sabljic, A. *J. Phys. Chem. A* **1997**, *101*, 4245−4253.

aug-cc-pVQZ) and 19.57 kcal/mol (CCSD(T)/aug-cc-pVTZ)[71] and 18.46 kcal/mol (MP2−R12/aug-cc-pV(T/Q)Z).[72] The MP2/6-311++G(3df, 3dp) and MP2−R12/aug-cc-pV(T/Q)Z barrier heights for the tetramer (12.73 vs 12.32 kcal/mol) and pentamer (12.57 vs 12.63 kcal/mol) also agree quite well. We did not consider the application of counterpoise corrections for the improved description of the individual monomers in the complex by the basis functions of the other monomers: Already for the determination of the stabilization energy of the clusters under consideration a counterpoise correction would have to be interpreted with special care.[73,74] Moreover, for the hydrogen rearrangement considered in this study the supermolecular picture completely loses its significance. Especially the tetramer and the pentamer have to be considered as one single molecule that undergoes an intramolecular rearrangement.[37] For the transition state the concept of monomers, which are improved in their electronic descriptions by basis functions of other monomers, also loses its significance. Any definition of monomers in the transition state is arbitrary. Further, a counterpoise correction of the transition state would be completely dominated by the monomer relaxation contribution.[75] It is mathematically obvious that the counterpoise corrected result converges (not necessarily faster[74]) to the same value as the uncorrected one in the limit of infinite basis set, if there were no fragment relaxation. This still can be assumed to be valid, if the fragment relaxation is small. Significance, accuracy, and most important the proper convergence of a counterpoise corrected energy barrier has to be doubted if the fragment relaxation becomes large, as in the case for the transition state of the concerted neutral hydrogen exchange in cyclic hydrogen fluoride clusters. Therefore, we rather rely on barrier estimates gained with large basis sets. Quite low T1 diagnostics of both the minima and the transition state[6,71] (0.0106 for the minima and 0.0115 for the transition state at CCSD(T)/aug-cc-pVTZ level) clearly indicate that a multiconfiguration treatment is not needed[76,77] and that already MP2 calculations using large basis sets can provide reasonable barrier estimates as is also indicated by the aforementioned benchmark calculations.

As the zero-point corrected MP2/6-311++G(3df,3dp) barrier height (16.0 kcal/mol) is grossly overestimated by PM3 (60.2 kcal/mol) and AM1[78] (104.7 kcal/mol), it is evident that specific reaction parameters are needed for the correction of these deficiencies. AM1 even fails to reproduce the correct number of "imaginary" frequencies in the D_{3h} structure (3 instead of one), and some frequencies are prone to an error of more than 100% in magnitude. PM3 performs considerably better, since it describes the TS structure qualitatively right as a first-order saddle point. In $(HF)_3$ therefore all 17 nonderived[46,47] PM3 parameters were adjusted for a reproduction of 6 geometrical quantities, 24 vibrational frequencies, the barrier between C_{3h} and D_{3h} structures, and its zero-point corrected analogue. This task to reproduce geometry, electronic information, and reaction energetics at the same time has been considered to be "perhaps impossible".[41,79] With the intention of finding a single set of parameters for all existing HF oligomers, all 17 parameters were reassigned, in order not to destroy the high interdependencies and not to lose flexibility. It appeared to be impossible to find such a set for all three oligomers simultaneously, mainly due to the varying and steep valleyed nature of the PES for the different number of monomers. From semiempirical theory it is quite clear that the effects of parameter changes are in no way additive or even systematic.[46] This is the reason why the Hamiltonian had to be reassigned with an optimizer like a genetic algorithm. The impact of genetic algorithms on chemistry has grown enormously in the last years.[49,80−82]

Table 1. Optimized PM3 Specific Reaction Parameters[a]

parameter	atom	$(HF)_3$	$(HF)_4$	$(HF)_5$	standard PM3
U_{ss}	F	−135.084005	−141.074	−137.399	−110.435303
U_{pp}	F	−94.748699	−111.125	−108.608	−105.685047
ζ_s	F	4.398730	3.46312	3.47866	4.708555
ζ_p	F	2.203690	1.9647	1.87568	2.491178
G_{ss}	F	11.509987	12.0691	11.8662	10.496667
G_{sp}	F	14.987400	12.5312	15.206	16.073689
G_{pp}	F	13.226399	17.9397	15.6197	14.817256
G_{p2}	F	12.761100	15.4722	14.3586	14.418393
H_{sp}	F	0.767448	0.713225	0.800721	0.727763
α	F	3.375850	3.23358	3.37126	3.358921
β_s	F	−63.295196	−55.6631	−47.3701	−48.405939
β_p	F	−34.584496	−33.5636	−34.394	−27.744660
U_{ss}	H	−10.992701	−16.1833	−13.4493	−13.073321
ζ_s	H	0.870627	0.941573	0.88933	0.967807
β_s	H	−7.237549	−4.06517	−4.07835	−5.626512
G_{ss}	H	11.737696	13.7746	13.7331	14.794208
α	H	4.086760	4.0733	4.0889	3.356386

[a] α = core−core repulsion integral in $Å^{-1}$, β = resonance integral in eV, ζ = slater exponent in au, U = one-center core electron attraction in eV, G = two-electron one-center repulsion integral in eV; indices correspond to atomic orbitals.

3.2. Implementation. We minimized the sum of weighted root-mean-square deviations of all configurations with a genetic algorithm, using a uniformly distributed starting generation of 130 individuals, 24 bits per parameter (making a total genome length of 408 bits), a crossover rate of 0.6, a mutation rate of 0.001, and a σ selection with a scaling factor of 2.0. The parameter optimization algorithm stopped when one of the two following termination criteria had been fulfilled: The first one was simply that in the evaluation of 20 successive generations, no new best candidate solution is found. Second, exceeding the maximum bias of 95% converged genes (a converged gene is a gene that is found in 95% of all individuals in the current generation) also led to an output of the best candidate and thus ended the calculation. Further, a constraint of allowing a maximal deviation for each individual parameter of 32% in any direction was imposed. The use of the elitist operator or user selected initial populations only improved convergence, but did not lead to a better guess for the optimal parameter set.

The obtained set of parameters was used as a starting vector for a Levenberg−Marquardt[58] algorithm, which smoothly switches between steepest-descent and Newton−Raphson search, to find a point with zero gradient. This local extremization method changed the pre-optimized parameters at most by 0.1%. Therefore, we concluded that the genetic algorithm alone is sufficient and applied the same strategy for all other oligomers, omitting the step of local refinement.

3.3. Resulting Parameters. In Table 1 the found sets of PM3 specific reaction parameters are shown. Some parameters deviate only in one direction from the standard PM3 value and reach nearly the same value (like α(H), U_{ss}(F), or β_p(F)) for all oligomers, demonstrating their physical significance and their specificity for the HF clusters. We consider them as the most important ones for agreement with the ab initio data. Others remain near the PM3 standard value (like ζ_s(H), H_{sp}(F), or α(F)). Eventually, they could be omitted completely in the parameter optimization. Other PM3 parameters, which oscillate around the standard value (like U_{pp}(F), G_{pp}(F), G_{p2}(F), U_{ss}(H), or β_s(H)), seem to play a minor role for reaching the aimed configurations and could be omitted as well. An attempt to accommodate a single set of 17 parameters to properties of all 3 oligomers failed in reproducing the 6

(71) Liedl, K. R.; Xantheas, S. S.; Rode, B. M.; Dunning, T. H., Jr. To be submitted for publication.
(72) Klopper, W.; Quack, M.; Suhm, M. A. *Mol. Phys.*, in press.
(73) Schwenke, D. W.; Truhlar, D. G. *J. Chem. Phys.* **1985**, *82*, 2418−2426.
(74) Liedl, K. R.; Sekusak, S.; Mayer, E. *J. Am. Chem. Soc.* **1997**, *119*, 3782−3784.
(75) Xantheas, S. S. *J. Chem. Phys.* **1996**, *104*, 8821−8824.
(76) Lee, T. J.; Taylor, P. R. *Int. J. Quantum Chem.* **1989**, *23*, 199−207.
(77) Lee, T. J.; Rice, J. E.; Scuseria, G. E.; Schaefer, H. F., III *Theor. Chim. Acta* **1989**, *75*, 81−89.
(78) Dewar, M. J. S.; Zoebisch, E. G.; Healy, E. F.; Stewart, J. J. P. *J. Am. Chem. Soc.* **1985**, *107*, 3902−3909.
(79) Truong, T. N. *J. Chem. Phys.* **1994**, *100*, 14−25.
(80) Mestres, J.; Scuseria, G. E. *J. Comput. Chem.* **1995**, *16*, 729−742.
(81) Clark D. E.; Westhead D. R. *J. Computer-Aided Molecular Design* **1996**, *10*, 337−358.
(82) Judson, R. Genetic Algorithms and Their Use in Chemistry. In *Reviews in Computational Chemsitry;* Lipkowitz, K. B., Boyd, D. B., Eds.; VCH Publisher, Inc.: New York, 1997; Vol. 10, pp 1−73.

Table 2. Structures, Frequencies, and Energetics (distances in Å, angles in deg, frequencies in cm^{-1}, and energies in kcal/mol) from Calculations with the Optimized Parameter Sets, the Standard PM3 Sets, and the MP2 Reference Method[37,24]

	PM3	PM3-SRP	MP2/ 6-311++G(3df,3dp)
		Trimer	
barrier	72.9	24.9	18.7
corr barrier	60.2	14.9	16.0
$(FF\text{-}dist)_{Min}$	2.472	2.556	2.612
$(FF\text{-}dist)_{TS}$	2.128	2.238	2.242
$(FH\text{-}dist)_{Min}$	0.953	0.993	0.933
$(FH\text{-}dist)_{TS}$	1.149	1.155	1.152
$(HFF\text{-}angle)_{Min}$	34.1	13.3	21.5
$(HFF\text{-}angle)_{TS}$	22.2	14.4	13.2
$(freq)_{Min}$	193.1−4191.7	448.4−4001.5	190.0−3892.7
$(freq)_{TS}$	489.6−1985.2	477.0−2397.9	566.6−2117.1
$(freq)_{imag}$	2605.1i	1539.3i	1733.3i
		Tetramer	
barrier	76.6	17.4	12.7
corr barrier	64.1	4.9	8.0
$(FF\text{-}dist)_{Min}$	2.565	2.596	2.516
$(FF\text{-}dist)_{TS}$	2.149	2.389	2.265
$(FH\text{-}dist)_{Min}$	0.952	1.051	0.946
$(FH\text{-}dist)_{TS}$	1.114	1.203	1.138
$(HFF\text{-}angle)_{Min}$	23.6	10.2	9.4
$(HFF\text{-}angle)_{TS}$	15.2	7.0	5.8
$(freq)_{Min}$	36.4−4262.3	38.9−3663.8	46.3−3699.6
$(freq)_{TS}$	75.5−2383.1	46.6−1683.2	72.9−2111.0
$(freq)_{imag}$	1871.5i	1386.2i	1498.0i
		Pentamer	
barrier	91.2	17.9	12.6
corr barrier	76.4	2.5	6.5
$(FF\text{-}dist)_{Min}$	2.604	2.600	2.484
$(FF\text{-}dist)_{TS}$	2.171	2.390	2.264
$(FH\text{-}dist)_{Min}$	0.951	1.058	0.950
$(FH\text{-}dist)_{TS}$	1.105	1.198	1.132
$(HFF\text{-}angle)_{Min}$	18.1	5.6	3.7
$(HFF\text{-}angle)_{TS}$	10.7	3.9	1.7
$(freq)_{Min}$	36.3−4290.4	28.7−3576.5	26.7−3611.9
$(freq)_{TS}$	62.7−2503.3	21.8−1754.1	37.2−2111.3
$(freq)_{imag}$	1614.8i	1217.4i	1431.3i

barriers and 3 "imaginary" frequencies of the 3 systems simultaneously with a higher precision than 20%.

In Table 2 the reproduction of configurations for all oligomers is given. For a better overview, only the "imaginary" frequencies and the lowest and highest real ones are given for the aimed for MP2/6-311++G(3df,3dp) and the original PM3 frequencies as well as for the PM3-SRP case. The FF distance therein is defined as the shortest distance between neighboring fluorine atoms, the FH distance is defined as the distance from one hydrogen to the next fluorine atom, and the HFF angle is defined as the angle measured from the midstanding hydrogen to its nearest fluorine and finally to the other fluorine neighbor. It serves as a measure for hydrogen bond linearity (cf. Figures 1 and 2). The PM3-SRP approach provides an enormous improvement over the original PM3 method concerning barrier height, high-energy frequencies, and "imaginary" frequencies. The geometric predictions were improved especially concerning the angles. It was not possible to compensate for the deficiencies of the semiempirical model to describe geometric trends with cluster size (especially the minimum FF distance) appropriately. Nevertheless, the PM3-SRP geometries seem to be reasonable, looking at the magnitude and sign of errors in bond lengths and angles for each individual species. Both pentamer extrema only seem to be increased in size by 4−6%, but maintain the correct relative arrangement, as can be seen from the angles. Similarly, 4−6% apply to the tetramer extrema. For the trimer, the TS structure coincides perfectly with the MP2 geometry, whereas the minimum is 8° distorted due to a 0.06 Å elongated FH distance. We believe that these deficiencies are small enough for obtaining a reliable hydrogen exchange rate.

4. Energetics and Dynamics

4.1. Reaction Path. There is little doubt nowadays that the hydrogen exchange mechanism between fluorine neighbors is of a concerted rather than stepwise nature.[5,6,24,36,37] Other tunneling pathways via ionic intermediates can presumably be excluded, because NMR spin doublet coalescence can be suppressed in carefully neutralized liquid HF.[27,72] An analysis of the angles between the gradient on the MEP and the "imaginary" modes of the transition states showed in a previous study[24] that the reaction path is dominated by the HF stretching normal mode in the region of the saddle point, whereas beginning between 0.5 and 1.0 Bohr (using a reduced mass $\mu = 1$ amu) away from the saddle point, this rapidly changes to the symmetric FF stretching mode (cf. Figures 1 and 2 for the pentamer). Because the PES curvature is very large near the transition state on the ridge of the reaction swath,[24] the need for reliable LCT calculations is clearly demonstrated.

In summary, the picture of vibration assisted tunneling for the reaction process including large curvature via the D_{nh} TS is as follows: Starting from one minimum geometry, the heavy atoms approach each other following the FF stretching mode ("reaction-coordinate") accompanied by the HF bending mode ("vibrational assistance"). All hydrogens are transferred in the same direction and at the same time to the next F atom, before the heavy atom framework has reached its vibrationally most compact form ("tunneling"). Thus, instead of going over the barrier, the H atoms tunnel through the reaction swath with a high probability. Therefore the apparent activation energy[52,67] for the process is lower than the actual barrier height, which is reflected in the nonlinear Arrhenius plots in Figure 6. This tunneling event can occur far below the saddle point energy on straight line paths from one side of the swath to the other. For this reason, the term "direct corner cutting" is often used as a synonym for LCT. SCT pathways as well do not cross the saddle point on the MEP ("corner cutting"), but in contrast to the LCT case, the trajectories stay near the MEP.

4.2. Ridge of the Reaction Swath. As the LCT trajectories cross the PES on paths very far away from the MEP, the regions of interest on the surface span from the surrounding of the MEP to the reaction swath,[41,83,84] which can be found inbetween two MEP branches (from the TS to the first minimum and the TS to the second minimum). It is important to know the shape of the PES in this region, because one can estimate the probability of a trajectory passing through this region of the potential with its aid.

For a symmetric reaction path, as in the case investigated here, it is evident that information is best obtained in the middle between the two branches connecting TS and minima, i.e., where all hydrogens are forced to stay at the half angle between the two neighboring fluorine atoms and the heavy atoms are moved away from each other until their distance has reached the minimum geometry value. This strategy has been performed elsewhere,[24] but it has the deficiency that it cannot easily be extended to less symmetric or totally unsymmetric reactions.

Due to this deficiency, we here propose a more general, improved definition of the ridge of the reaction swath: The idea is to add both vectors pointing from the TS to the minima (see Figure 3). Mathematically speaking, each vector is represented by a number n of coefficients, where n is three times the number of atoms. These vectors are obtained by performing a basis set transformation of the Cartesian coordinates of both

(83) Truhlar, D. G.; Gordon, M. S. *Science* **1990**, *249*, 491−498.
(84) Liu, Y.-P.; Lu, D.-h.; Gonzalez-Lafont, A.; Truhlar, D. G.; Garrett, B. C. *J. Am. Chem. Soc.* **1993**, *115*, 7806−7817.

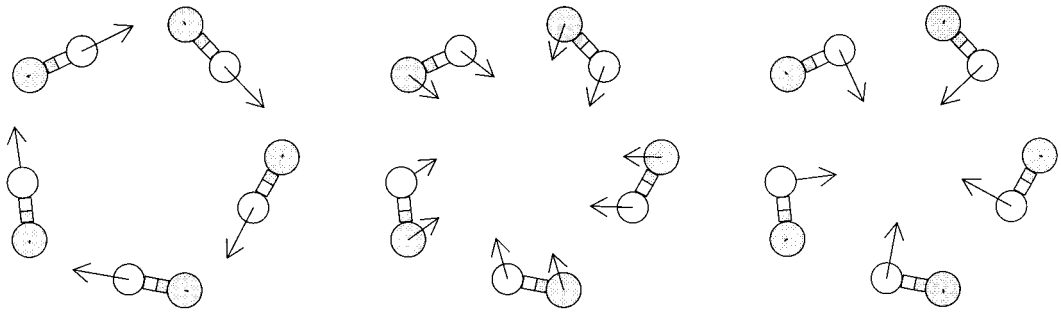

Figure 1. $(HF)_5$ minimum normal modes: symmetric HF stretching, symmetric FF stretching, and symmetric HF bending.

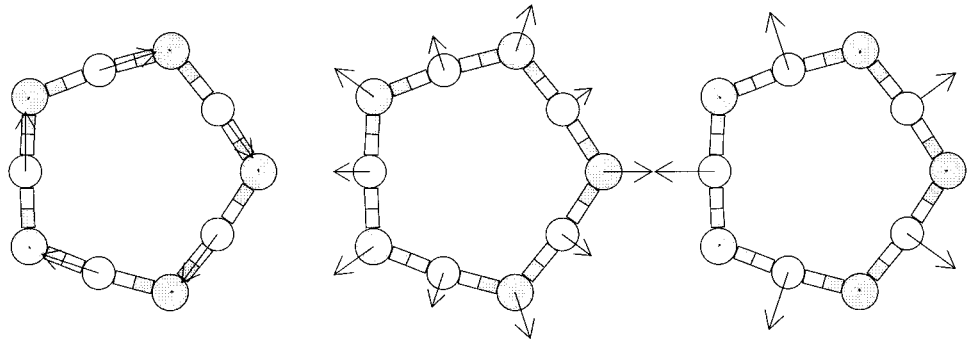

Figure 2. $(HF)_5$ transition state normal modes: symmetric HF stretching, symmetric FF stretching, and symmetric HF bending.

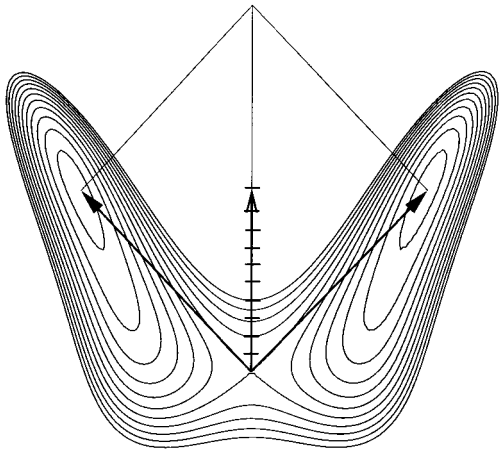

Figure 3. Simplified two-dimensional PES of $(HF)_5$ showing the vector from the transition state (in the middle) to the first minimum (top left), the transition state to the second minimum (top right), and the "ridge vector" of the reaction swath with 10 points on it, where single-point energies were calculated. On the contour plot, abscissa and ordinate represent symmetric HF stretching and FF stretching, respectively.

minima to the transition states normal mode basis.[36] All rotations and translations have to be removed beforehand and therefore have zero coefficients. These two sets of $(n - 6)$ coefficients (i.e., one number for each vibration) or in other words these two vectors imply the distance one has to proceed along each TS-vibration direction in order to reach the first or the second minimum, respectively. To arrive at the point in the middle of the line connecting both minima, which is the final point on the ridge, one has to add the two vectors (i.e., the corresponding coefficients) to get the "ridge vector". Now, the improved definition of the ridge of the reaction swath is to follow this "ridge vector" in different fractions reaching from 0 (i.e., the TS itself) to 0.5 (i.e., the structure between the two minima). We calculated 11 equally spaced (i.e., fractions of 0.05) single point energies, as indicated in Figure 3. The final point on the ridge vector is far away from all three extrema and, therefore, the ab initio description here has only a minor influence in the interpolation procedure. Hence, a good description of PM3-SRP at this point is as well needed to generate a reliable PES for all relevant regions in a LCT calculation.

For the HF clusters the multidimensional picture is reduced to a two-dimensional picture due to the facts that (a) all asymmetric normal modes must have zero coefficients to retain the reaction symmetry and (b) from the remaining three modes, the one corresponding to the "imaginary" frequency has the same coefficient, but with opposite sign for the two minima and, therefore, cancels out upon addition of both vectors. The two remaining modes correspond to the FF stretching and the in-plane HF bending mode (cf. Figure 2). This demonstrates the high symmetry of the reaction, i.e., only 2 out of 30 normal modes are relevant for the ridge of $(HF)_5$. (Note that these two modes are represented as only one dimension in Figure 3.) The former[24] and this improved definition of the ridge are identical, with the exception that the hydrogens are not relaxed in the direction of the TS's symmetric bending mode (cf. Figure 2).

In Table 3 the coefficients of one minimum in the basis of the transition states' normal modes in comparison between ab initio and semiempirical methods are given. The minimum and transition structures as well as the normal modes were all taken from the specified computational method. The differences in these coefficients can mainly be attributed to the problems of semiempirical methods to reproduce MP2 geometries. For example, in the case of the pentamer the coefficient for the bending mode is higher, reflecting the fact that the changes between TS and minimum are larger for PM3-SRP than for MP2. Without specific reaction parameters, PM3 completely fails to describe essential features of the reaction as can be seen with the aid of the TS's normal mode basis. Therefore, evidence is given again that specific reaction parameters are necessary. This is especially obvious in the case of the symmetric HF bending mode coefficient of $(HF)_5$. The PM3 coefficient is more than 13 times larger than the MP2 coefficient. This means

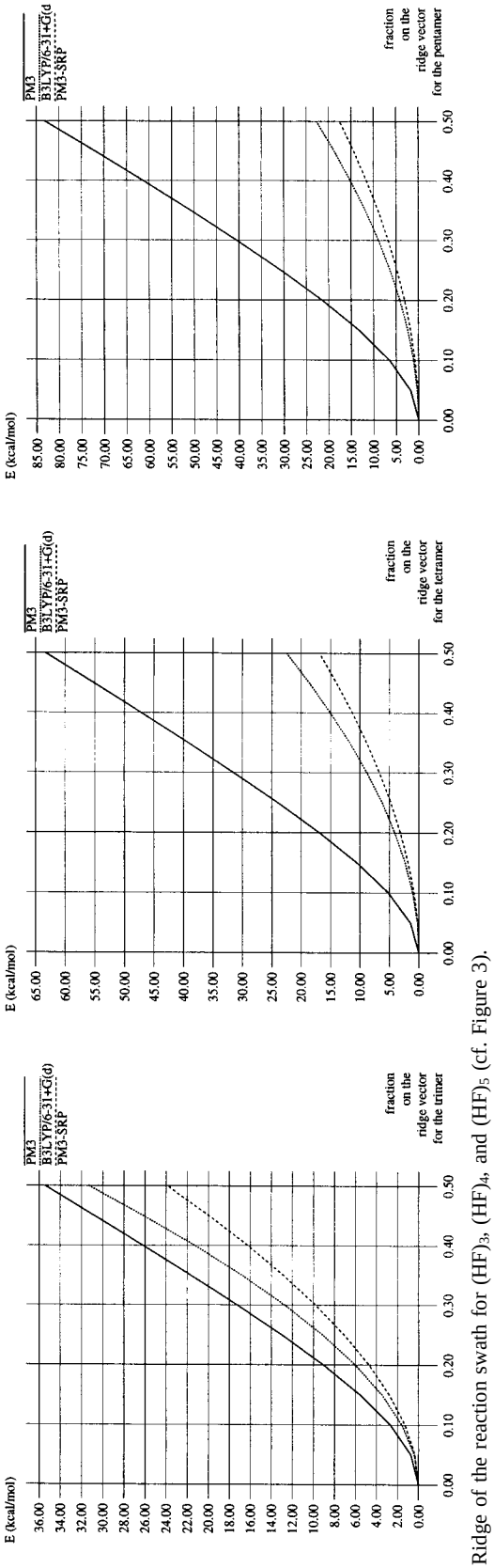

Figure 4. Ridge of the reaction swath for $(HF)_3$, $(HF)_4$, and $(HF)_5$ (cf. Figure 3).

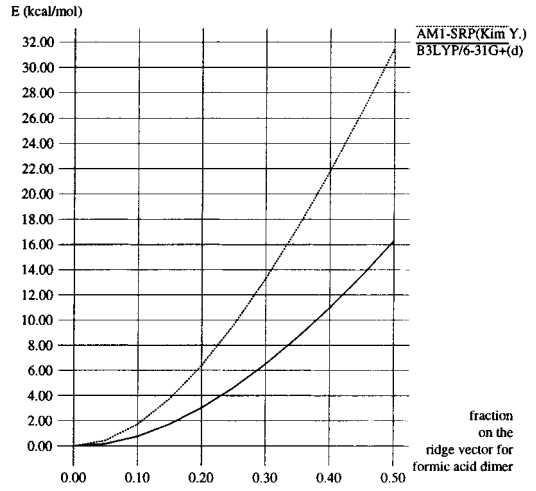

Figure 5. Ridge of the reaction swath for the formic acid dimer calculated at the B3LYP/6-31+G(d) and the AM1-SRP[12] levels of theory.

that PM3 is unable to describe the reaction correctly, as its geometry description and normal mode data are insufficient. From a mere PM3 analysis, one would conclude that following the symmetric HF bending mode is a vital part in the pentamer's hydrogen exchange reaction. But according to MP2, this normal mode hardly plays a role in the description of the interconversion from the TS to a minimum. Also the coefficient for the symmetric HF stretching mode, which is a direct measure for the barrier width, is increased by more than 30% in going from MP2 to PM3 description. Tunneling becomes a less probable event by using the PM3 Hamiltonian, by which the barrier width is increased by one-third. For PM3-SRP the picture resembles much more the MP2 characterization than the pure PM3 one. The normal modes, the corresponding frequencies, especially the higher frequencies, and their coefficients seem to be reasonable in comparison to MP2 and thus a proper description of tunneling events is feasible.

Looking at Figure 4, it is obvious that the height of the ridge is strongly overestimated for the less strained oligomers at the PM3 level and, therefore, does not allow the calculation of reasonable LCT transmission coefficients κ^{LCT} at this level of theory. Due to this incorrect description of the reaction swath and due to the too broad barrier (as discussed above), the MP2///PM3 (without SRP) results in a former study[24] were about the same for inclusion of SCT and LCT in $(HF)_3$ and $(HF)_4$, implying that the system has no opportunity to cut the corner far away from the TS. For $(HF)_4$, the ridge rises steeply and reaches an energy difference of 64 kcal/mol (instead of 22 kcal/mol), and hence suggests that the LCT treatment cannot provide a further enhancement of SCT rate constants. For $(HF)_3$, the MP2///PM3 (SCT) rate constants were found to be considerably higher than those obtained with the MP2///B3LYP (SCT) treatment.[24] This deficiency is corrected by the use of MP2///PM3-SRP, confirming our parametrization. Therefore, our treatment using PM3-SRP allows a proper description of both SCT and LCT effects, as the parametrization of the semiempirical method not only reproduces the barrier height and width for all clusters, but also provides a solid picture for the description of the reaction in terms of all essential vibrations. Especially the coefficient for the symmetric HF-bending mode shows a considerable improvement over the mere PM3 calculation. It is obvious that the SCT treatment has to be appropriate, before starting to consider LCT. For $(HF)_3$ the importance of PM3 reparametrization lies therefore not mainly in the better

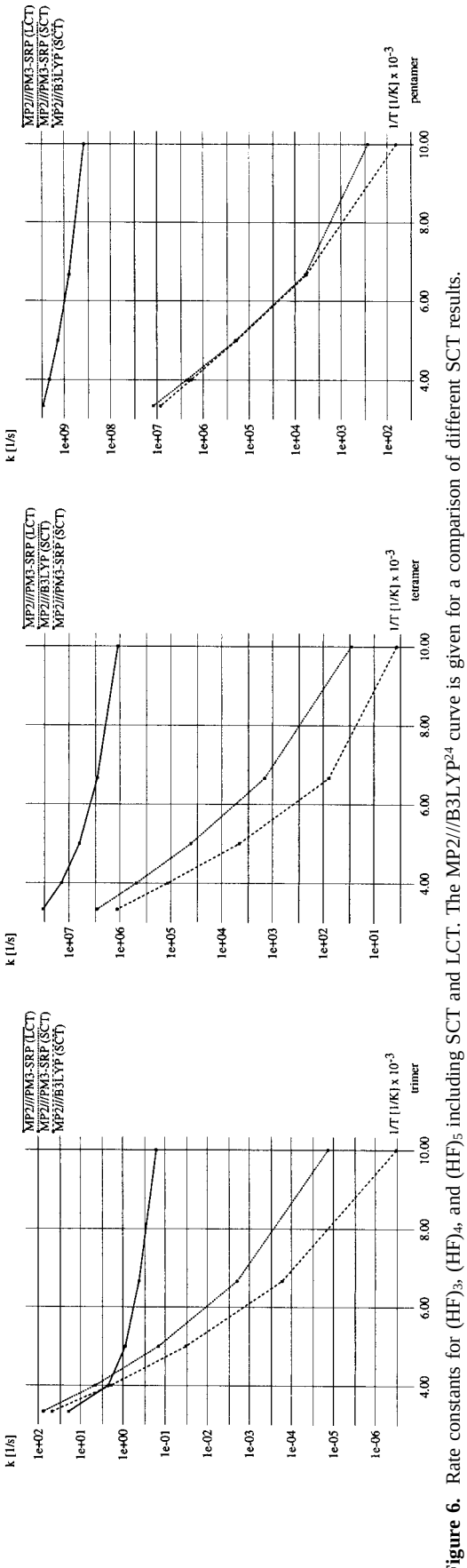

Figure 6. Rate constants for $(HF)_3$, $(HF)_4$, and $(HF)_5$ including SCT and LCT. The MP2//B3LYP[24] curve is given for a comparison of different SCT results.

Table 3. Non-Zero C_{nh} Coordinates in D_{nh} Normal Mode Basis

	MP2/ 6-311++G(3df,3dp)	B3LYP/ 6-31+G(d)	PM3-SRP	PM3
	Trimer			
symm HF stretch	0.74	0.67	0.53	0.75
symm FF stretch	0.38	0.31	0.32	0.36
symm HF bend	0.27	0.21	0.08	0.49
	Tetramer			
symm HF stretch	0.63	0.58	0.51	0.79
symm FF stretch	0.40	0.34	0.31	0.66
symm HF bend	0.15	0.13	0.19	0.94
	Pentamer			
symm HF stretch	0.63	0.59	0.53	0.85
symm FF stretch	0.52	0.46	0.44	0.86
symm HF bend	0.09	0.08	0.18	1.20

description of the ridge of the reaction swath or the barrier width compared to PM3, which were already good enough. It rather has to be seen in the much better agreement between both SCT curves in Figure 4 (the MP2///PM3 (SCT) curve reaches from $k(100\text{K}) = 8.5 \times 10^3\ \text{s}^{-1}$ to $k(300\text{K}) = 4.1 \times 10^5\ \text{s}^{-1}$).[24]

The PM3 agreement for the trimer's ridge could be ascribed to a fortuitous cancellation of errors. The error might be due to a bad energetic description of the H-bond and a bad description of ring strain having opposite sign and incidentally the same amount. This fortuitous removal of error is lost partly at the PM3-SRP level, but here the weakness should be of a systematic nature rather than accidental. Nevertheless, for the 4- and 5- (heavy-atom) membered rings, the PM3-SRP Hamiltonian improves the description on a scale of about 50 kcal/mol (ca. 300%) at the upper limit of the ridge of the reaction swath.

For the formic acid dimer Kim published a set of nine specific reaction parameters to the AM1- Hamiltonian (AM1-SRP) for a direct semiempirical dynamics calculation (single-level).[12] The PES is very similar to those of the hydrogen fluoride clusters, especially to that of $(HF)_5$. This can be seen in Figure 5, where the ridge is of an equally harmonic shape and of comparable height, and from the calculated barriers (zero-point corrected values in brackets), being 8.9 (5.2) kcal/mol for formic acid dimer and 12.6 (6.5) kcal/mol for the cyclic pentamer of HF. The best estimates for the electronic binding energy per hydrogen bond of 8.1 kcal/mol[74] for formic acid dimer and 7.7 kcal/mol[37] in the case of $(HF)_5$ underline this high similarity. Further, only 4 out of the formic acid dimer's 30 normal modes are relevant for the description of the ridge, indicating a similar high symmetry.

4.3. Reaction Rate Constants. For heavy−light−heavy atom combinations, which can be found in the surveyed clusters in repetitive units, the PES is strongly curved.[52] Therefore state-of-the-art rate constants can only be obtained by inclusion of large curvature tunneling. Dual-level dynamics (i.e., VTST-IC), using ab initio calculations alone, suffer from the disadvantage that no LCG3 calculations can be afforded to include multidimensional semiclassical tunneling paths, because the additionally necessary information for the reaction swath would consume a multiple of the resources needed for the whole SCT calculation. It is therefore necessary to provide a lower-level PES for calculations including LCT. However, for a reliable LCT description, the SCT rate constants of the ab initio/// semiempirical calculations should be similar to SCT results, where interpolated corrections are evaluated at the ab initio level of theory.

For this reason, the SCT rate constants obtained with the centrifugal-dominant small curvature semiclassical adiabatic

ground-state method (CD-SCSAG) and triple slash dynamics at the MP2/6-311++G(3df,3dp)///B3LYP/6-311++G(3df,3dp) level of theory were compared with CD-SCSAG results obtained at the MP2/6-311++G(3df,3dp)///PM3-SRP level and found to coincide reasonably, as can be seen in Figure 6. Further, it can be seen in this figure that the linear Arrhenius behavior is completely lost at low temperatures (going to the right sides in Figure 6), which is due to nonclassical tunneling.

The most important feature in this figure is the vast amount of increase in reaction rates due to large curvature tunneling (LCT) effects found by applying the LCG3 method. The curvature of the LCT line compared to the SCT lines is raised considerably and the increased tunneling activity leads to rates 4, 5, and 6 orders of magnitudes higher at 100 K for $(HF)_3$, $(HF)_4$, and $(HF)_5$, respectively. In the case of the pentamer all 5 hydrogens swap their fluorine partners nearly a billion times per second already at a temperature near that of liquid nitrogen. Even at room temperature or higher a significant increase in the exchange rate can be found for the tetramer and even more so for the pentamer, for which the rate becomes the 240-fold of the SCT result at 300 K by including LCT. For the tetramer, the apparent Arrhenius activation energy[52,67] is reduced compared to pure TST treatment by 2.3 kcal/mol at 300 K and 5.4 kcal/mol at 100 K.

For formic acid dimer, Kim[12] performed similar calculations in a highly interesting study and found an increase from 4.34 $\times$ 10^7 s^{-1} (SCT) to 6.28 $\times$ 10^8 s^{-1} (LCT) at 300 K using a single-level AM1-SRP approach. This is about an order of magnitude lower than the experimental results of various carboxylic acid dimers suggest. We found an increase in reaction rate constants of more than 2 orders of magnitude for the cyclic pentamer of HF at 300 K, where the ridge is reproduced very well by PM3-SRP. Probably, the rate constant given by Kim[12] could be refined further to higher numbers. The AM1-SRP ridge in Figure 5, which is about twice as high as the ab initio height at its final point, reveals that direct corner cutting effects are very likely to be underestimated. The barrier width is overestimated, looking at the basis-transformation coefficient from the normal mode with "imaginary" frequency (0.69 for AM1-SRP and 0.55 for Becke3LYP/6-31+G(d)) and, therefore, shows that the amount of tunneling is again underestimated. For benzoic acid, which is thought to be very similar to formic acid concerning hydrogen exchange,[85] the inverse correlation time τ_c^{-1} has been estimated by field cycling NMR via measurement of nuclear spin−lattice relaxation time T_1.[14] Brougham et al. found the rate constant $k = 8 \times 10^{10}$ s^{-1} at 300 K, which coincides with our opinion that Kim's[12] exchange rates could be an order of magnitude too low and that the estimated time scale for hydrogens swapping heavy-atom partners of slightly less than a nanosecond is reliable, for both formic acid dimer and $(HF)_5$. Earlier studies[11] showed that this time scale for carboxylic acid dimers is nearly independent of substitution, as the rate constants for three different deuterated carboxylic acid dimers are found to agree within a factor of 2 at 300 K (2.5×10^9 s^{-1} to 5.2×10^9 s^{-1}).

5. Conclusions

We analyzed in detail the mechanism of the reactive pathway converting clockwise "isomers" of cyclic hydrogen fluoride clusters into counterclockwise isomers, as we hoped that our calculations can help to encourage further experimental work using NMR and FTIR spectroscopy, which should confirm the presented results. We believe that the major problem, why such studies have not been published yet, is the abundance of various stable clusters of different size in HF vapor.[1,2,5] Nevertheless, we are rather sure that effects such as tunneling splittings, which have already been estimated by measurements in benzoic acid dimer crystals for the symmetric limit (0.32 cm^{-1})[86] and for asymmetric carboxylic acid dimers in the gas phase (0.5−5.0 cm^{-1}),[87] could in principle be found for the HF complexes, as the barrier height and width and the shape and height of the ridge of the reaction swath are very similar, especially for $(HF)_5$ and the formic acid dimer. In addition, rate constants such as the ones presented here should be measurable by means of nuclear magnetic resonance spectroscopy.

The calculation of concerted hydrogen exchange rate constants, especially at low temperatures, but also at room temperature or even higher, can only be reliable if large curvature effects are included. Nowadays, this can only be achieved within affordable time and with reasonable results by using specially parametrized low-cost methods, like PM3-SRP, or an appropriate analytic potential for interpolation between high-level stationary points. The reaction rates are increased up to 6 orders of magnitude at 100 K with the presented triple-slash approach in comparison to previously published results.[24] This shows that treatment with SCT is insufficient to provide even a crude estimate of rates. For methods neglecting multidimensional tunneling completely, at least at temperatures up to 300 K, the picture is in fact worse than that. The enhancement of rate constants can still be more than 2 orders of magnitude at room temperature.

The improved definition of the ridge of the reaction swath and the discussion of basis-transformation coefficients itself should help in understanding, why and how much reaction rates differ in going from methods ignoring multidimensional tunneling to SCT and further to LCT approaches. This provides a theoretical basis capable of estimating or explaining experimental results.

The high similarity of the hydrogen bond characteristics of the cyclic hydrogen fluoride pentamer to those of the dimer of formic acid in combination with the large amount of reliable experimental data for carboxylic acid dimers ensures us that our estimate of the rate constant $k(300K) = 2.8 \times 10^9$ s^{-1} for $(HF)_5$ is realistic and gives hope that it will be confirmed experimentally.

Acknowledgment. The authors are grateful to Martin A. Suhm for helpful discussion and comments on the manuscript.

JA972799T

(85) Bountis, T., Ed. *Proton Transfer in Hydrogen-Bonded Systems*; Vol. 291 of NATO ASI Series; Plenum Press: New York, 1992.

(86) Pierre, M.; Trommsdorff, H. P.; Hochstrasser, R. M. Optical studies of proton tunneling and relaxation in benzoic acid. In *Quantum Aspects of Molecular Motion in Solids*, Heidemann, A., Magerl, M., Prager, M., Richter, D., Springer, T., Eds.; Vol. 17, *Proceedings in Physics*; Springer: Berlin, 1987; pp 186−191.

(87) Costain, C. C.; Srivastava, G. P. *J. Chem. Phys.* **1964**, *41*, 1620−1627.